Impurity Transport in Internal Transport Barrier Discharges on JET

R. Dux[1], C. Giroud[2], K.-D. Zastrow[3], and JET EFDA contributors[4]

[1] *MPI für Plasmaphysik, EURATOM Association, D-85748 Garching, GERMANY*
[2] *FOM-Rijnhuizen, Ass. EURATOM-FOM, TEC, PO BOX 1207, 3430 BE Nieuwegein, NL*
[3] *EURATOM-UKAEA Fusion Association, Culham Science Centre, Abingdon OX14 3DB, UK*
[4] *See Annex1 in IAEA-FEC 2002,J.Pamela OV-1/1.4*
e-mail: Ralph.Dux@ipp.mpg.de

Abstract: Impurity behaviour in JET internal transport barrier discharges with reversed shear has been investigated. Metallic impurities accumulate in cases with too strong peaking of the main ion density profile. The accumulation is due to inwardly directed drift velocities inside the ITB radius. The strength of the impurity peaking increases with the impurity charge and is low for the low-Z elements C and Ne. Transport calculations show that the observed behaviour is consistent with dominant neoclassical impurity transport inside the ITB. MHD events in the core flatten the radial profile of the metallic impurity.

Introduction

Impurity accumulation occurs when the radial density profile of an impurity evolves a stronger peaking than the profile of the main plasma ion. This is usually observed in the central part of the plasma inside a normalised radius $r/a<0.5$. The high impurity concentration on axis leaves the main plasma impurity content nearly unchanged due to the small affected volume and vice versa the same impurity production at the vessel walls might produce largely different central impurity concentrations. The impurity sources are located in the edge region of the plasma and the equilibrium radial gradient of the impurity density n_I at radius r depends only on the ratio of the radial drift velocity v and the diffusion coefficient D at this radius: $(1/n_I)(dn_I/dr) = (\mathrm{v}/D)$. The diffusion coefficient has an anomalous and a neoclassical contribution D=D_{an}+D_{neo} and the convective transport, which is a necessary condition for impurity accumulation, is assumed to be purely neoclassical with v=v_{neo}. In a simplified treatment, only collisions of impurity and main ion D are considered and v_{neo} is for equal temperatures of both ion species $T_D = T_I$.

$$\mathrm{v}_{neo} = D_{neo}\frac{Z_I}{Z_D}\left(\frac{1}{n_D}\frac{dn_D}{dr} - H\frac{1}{T_D}\frac{dT_D}{dr}\right) \tag{1}$$

The density gradient term drives an inwardly directed convective flux, while the temperature gradient yields an outwardly directed drift velocity, where the factor H has typical values H=0.2–0.5. Thus, the normalised impurity density gradient is

$$\frac{1}{n_I}\frac{dn_I}{dr} = \frac{1}{n_D}\frac{dn_D}{dr}\frac{Z_I}{Z_D}\frac{D_{neo}}{D_{neo}+D_{an}}(1-H\eta_D) \tag{2}$$

where η_D denotes the ratio of the normalised temperature gradient to the normalised main ion gradient. Eq.2 shows, that impurity accumulation can only occur, if D_{an} is not too large compared to D_{neo} for plasmas with peaked ion density gradient at small η_D. In such a situation elements with higher charge number Z will accumulate stronger than low-Z elements. $D_{an} < D_{neo}$ is often observed in the central part of the plasma [1], however, sawtooth crashes periodically cause a flattening of the impurity profile. Plasmas with internal transport barrier (ITB) are thus of special concern with respect to impurity accumulation, since possible neoclassical inward convection is not suppressed by the low anomalous diffusive transport or by the sawtooth instability [2-6]. In low density ITB plasmas, the neoclassical inward drifts for the impurities can be provoked by the central fueling from the NBI heating, which creates peaked deuterium profiles for low D_{an}. In the following, impurity behaviour for ITB plasmas with reversed shear in JET will be described. Results on He transport investigations are given in [7], Ne transport in plasmas with and without reversed shear is compared in [8]. For monotonic shear ITB plasmas, complementary information on C and Ni can be found in [9] and on Ar in [10].

Data Analysis

Two soft X-ray (SXR) cameras with 250 μm thick Be filters (detection efficiency $>$0.1 for photons in the energy range 2.3-15 keV) served as the main diagnostic tool. The SXR cameras cover the plasma cross section with 35 vertical and 17 horizontal lines-of-sight and time averaged data with a time resolution of 1 ms were used. The measured radiation fluxes along the line-of-sights were unfolded by assuming constant emissivity ε_{sxr} on flux surfaces. The SXR emission was analysed to gain information about the impurity composition. The dependence of ε_{sxr} on the impurity density n_I and the electron density n_e can be written as

$$\varepsilon_{sxr} = \frac{n_e^2}{Z_D} L_D^{sxr} + n_e \sum_I n_I \left(L_I^{sxr} - \frac{Z_I}{Z_D} L_D^{sxr} \right). \qquad (3)$$

The first term gives the radiation for zero dilution while the second term contains the radiation caused by each impurity I including the dilution of the main ion D. For the plasma core, the mean charge Z and the total soft X-ray power coefficients L^{sxr} (including the detection efficiency of the setup) of each element can be calculated using corona ionisation equilibrium and thus are mainly functions of the electron temperature T_e. The relevant atomic data were taken from the ADAS database [11], while the detection efficiency was calculated from the tabulated coefficients of Henke [12]. Fig.1 gives an example for the unfolding procedure for discharge #53521. The high level of ε_{sxr} in the plasma centre can not be explained by low-Z impurities (Be – Ne) which mainly cause bremsstrahlung in the core. The strong emission must be due to the line radiation of metallic elements and Ni is assumed to be the predominant metallic impurity. The radiation from low-Z elements is calculated by taking the impurity densities of C and Ne (for discharges with Ne puffing) from CXRS and by increasing the C emission by 50% as an estimate for the contribution from other low-Z elements Be, N and F. Ni densities were calculated from the remaining difference $\Delta\varepsilon_{sxr}$=ε_{sxr}-$\varepsilon_{sxr,lowZ}$.

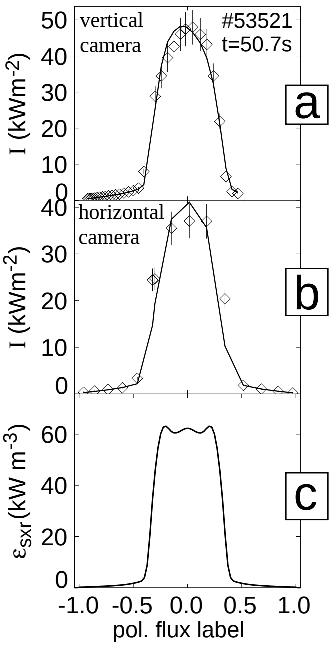

Fig. 1: *Measured radiation fluxes for two SXR cameras (a,b) and fitted local emissivity(c) for #53521 at t=50.7s. Calculated radiation fluxes from the fit are shown as a solid line (a,b).*

High Performance Discharges

The analysed high performance discharges had a current profile with strongly reversed shear and a central 'current hole' at the start time of the main heating power phase [13]. Fig.2 gives the evolution of C, Ne and Ni densities in discharge #51976 [14] with a high performance ITB of 1 s duration. Before the formation of the strong barrier, at t=45.8 s, T_i has an almost constant gradient length for the depicted radial range, and the impurity density profile is hollow or mildly peaked. A strong barrier in T_i, T_e and n_e forms at t$\approx$45.9 s. At t=46.2 s, the normalised T_i gradient is increased at a mid plane radius of $R\approx$3.5 m. The radius with increased normalised

T_i gradient shifts towards larger radii for the following time slices due to an expansion of the barrier width and due to the increasing Shavranov shift. For the later times, the radial region of the T_i barrier location is depicted by a vertical light grey bar. Inside that region T_i becomes progressively flat. Here, n_e and the impurity densities develop the strongest gradient and the radial region with increased density gradients is given by a darker grey bar. The impurity peaking increases with the impurity charge Z and is weakest for C and very strong for Ni. At t=46.9 s, the dominant Z_{eff} contribution is due to Ni and reaches a value of ΔZ_{eff}=1.5 for Z_{eff}=3.5 causing a dilution of $\Delta n_e/n_e$=6%. Thus, the n_i profile has not much reduced peaking compared with n_e.

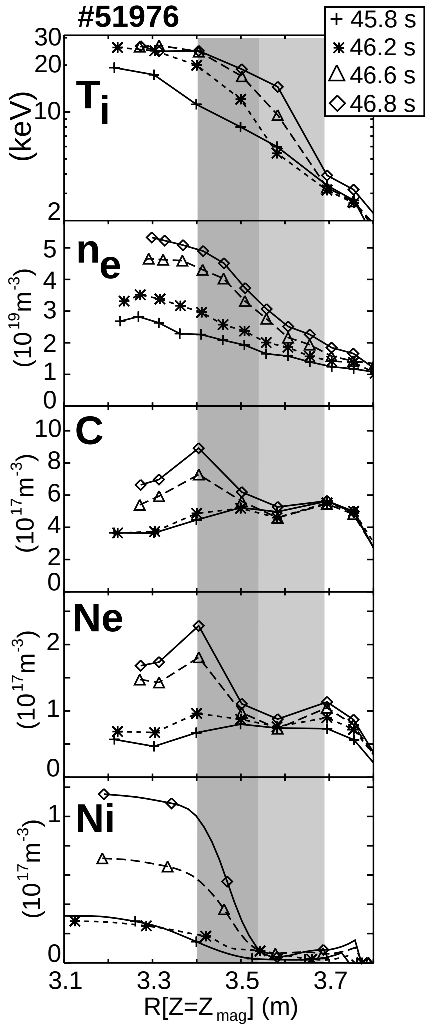

Fig.2: *Evolution of the radial profiles of T_i, n_e, n_C, n_{Ne} and n_{Ni} for the discharge #51976.*

The observed impurity accumulation is a pure transport effect due to convective particle flows. The radial transport of C, Ne and Ni has been simulated for #51976 with the impurity transport code STRAHL. In Fig.3, various profiles for three time points during the ITB phase t=46.2, 46.6, and 46.8 s are shown and compared with measurements. n_e(Fig.3a), T_i (Fig.3b), and T_e profiles were taken from the experiment. n_D follows from the impurity ion distributions and quasi neutrality. The classical, Pfirsch-Schlüter and banana-plateau contribution of the transport parameters were numerically evaluated by solving the coupled equations for the parallel velocities of a four component plasma (D,C,Ne,Ni) with NEOART [15-17]. using the fractional abundances of the different ion stages from the impurity transport code. D_{an}, which is assumed to be equal for all species, is set ad hoc. Close to the axis ($r\leq$0.2 m) the poloidal field becomes very low, the orbits of trapped particles are very large and standard neoclassical theory may not be applied. Here, the measured profiles are flat and a high value of D_{an}=1 m^2/s is used to describe this situation. For $r>$0.2 m, the anomalous diffusion coefficient is chosen to be below D_{neo} with D_{an}=0.02 m^2/s for radii inside the radius of the ITB and to increase from the ITB radius towards the edge. The radial evolution of the ITB radius is thus reflected in a broadening of the region with low D_{an} (see Fig.3c).

The simulation starts at t =45.8 s using radially constant impurity density with n_C=5$\times$10^{17}m^{-3}, n_{Ne}=7$\times$10^{16}m^{-3}, and n_{Ni}=1.5$\times$10^{16}m^{-3}. During the ITB phase, the neoclassical transport becomes increasingly convective with inwardly directed (negative) drift velocities in the radial region with weaker temperature gradient and pronounced electron peaking while in the region with strong temperature gradient v$_{neo}$ is close to zero or outwardly directed in the case of Ni. For Ne and Ni, the according diffusion coefficients D_{neo} are shown in Fig.3c while the ratio v$_{neo}$/(D_{neo}+D_{an}) is depicted in Fig.3d. The plot of v$_{neo}$/D demonstrates, that transport is more convective for Ni, the element with higher Z compared to Ne and stronger peaking is expected for Ni. This can be seen in Fig.3e and Fig.3f, where the siumlated density profile of Ni evolves a much stronger peaking than Ne. While the measured Ne densities are well described by the model, there is still not enough peaking of Ni in the simulation. The central density at t =46.8 s is n_{Ni}=8×10^{16}m^{-3}, i.e. 27% below the measured value. An artificial increase of the neoclassical drift of Ni by a constant factor of 1.4 yields a perfect match of measured and simulated profile evolution. When choosing the value of D_{an} inside the ITB a factor of 5 higher, i.e. D_{an}=0.1 m^2/s, the central Ni density rises only to n_{Ni}=6.4×10^{16}m^{-3} at t =46.8 s and an increase of the neoclassical drift by a factor of 1.8 is needed to fit the observed Ni peaking. Due to the uncertainties in the choice of D_{an} and in the measured gradients, it is difficult to quantify the goodness of the neoclassical transport description, however, there is certainly qualitative agreement between measured impurity evolution and the simulation, which assumes a dominating neoclassical transport.

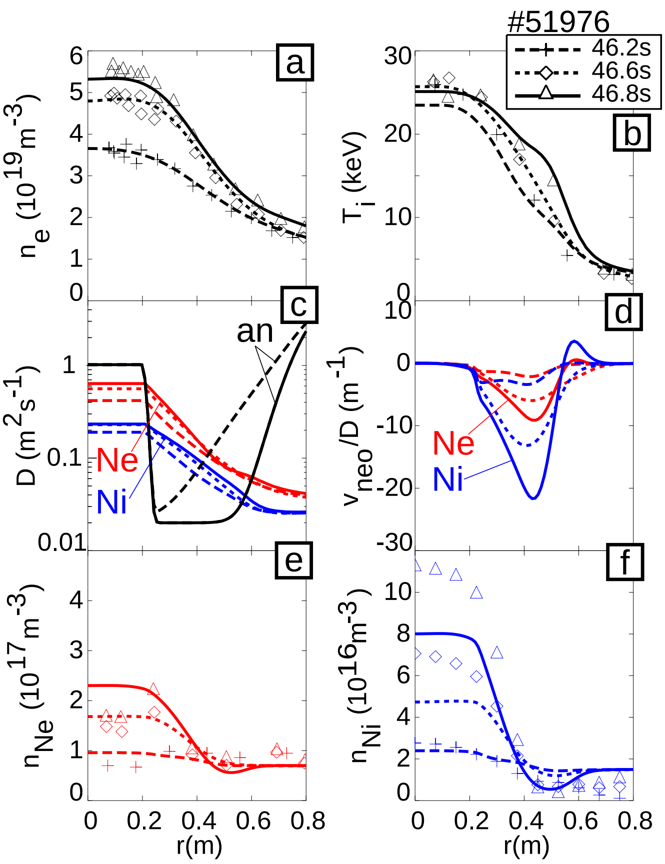

Fig.3: *Three radial profiles of n_e, T_i, D_{an}, D_{neo}, v_{neo}/D, n_{Ne} and n_{Ni} from the impurity transport simulation of discharge #51976. The overlayed symbols give experimentally measured profiles.*

Long ITB Discharges

In Fig.4 two reversed shear discharges (#53521 in black, #53697 in grey) with long ITB phases are compared [18,19]. The toroidal field is B_T=3.4 T. During the shown time interval, the plasma current has a constant value of I_p=2 MA for #53521 and I_p=1.8 MA for #53697 and in both discharges the plasma is heated with ≈15 MW of NBI and 3-5 MW of ICRH. LHCD is applied throughout the discharges. The total neutron rate is in the range 1.0-1.4×10^{16} s^{-1}. In #53521, the ITB in the ion channel is sustained for 27 confinement times.

The temperatures T_i and T_e and the Ni density n_{Ni} close to the plasma centre and at half radius are shown. Two horizontal interferometer channels (central, and half radius) give the evolution of the electron density profile. T_e and T_i are similar in both discharges with somewhat stronger gradients in #53521. The electron density, however, shows a pronounced difference and evolves a stronger peaking in #53521, where n_{Ni} becomes extremely peaked. The correlation between density peaking and Ni peaking can be understood in terms of neoclassical transport as discussed in the previous section. For #53521 at t≈50.7 s, the accumulated Ni is the dominant Z_{eff} contributor with central Z_{eff}=7 and the dilution due to Ni is $\Delta n_e/n_e$=20%. The central SXR emission ε_{sxr}=0.6×10^5 Wm^{-3} (see Fig.1) corresponds to a calculated local radiation loss of ε=1.4×10^5 Wm^{-3}, which is about the central heating power density into the electrons. Thus, the loss of confinement at t=51.1 s, which is very strong in the Ni channel, is probably a radiative collapse. The ITB reforms after this collapse [19], however, there is no information about the further evolution of Ni since SXR data collection stopped. MHD events, which lead to a sawtooth like signature of T_e, correlate with a decrease of the Ni peaking, which might become very strong as for #53697 at t=50.1 s, where the central radiation is too low to explain a radiative collapse. Here, a n=1-mode is observed, followed by a decrease of central plasma rotation by ≈30%, central electron density is lost and the Ni profile becomes flat. Further investigation is needed for these phenomena. Carbon density profiles from CXRS peak only slightly stronger as n_e and the concentration of C stays almost constant resembling the same Z dependence of impurity transport as in #51976.

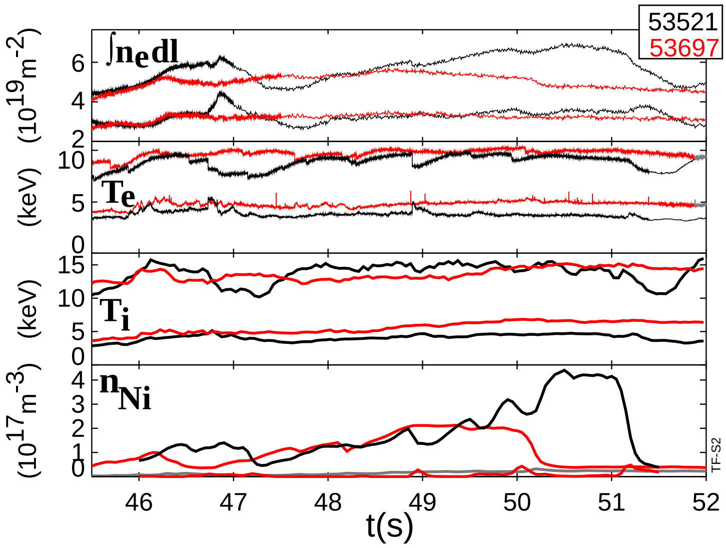

Figure 4: *Time traces for $\int n_e dl$, T_e, T_i and n_{Ni} for two reversed shear discharges (#53521 in black, #53697 in grey) with long ITB phases are compared.*

Conclusion

In ITB discharges with reversed shear, Ni accumulates in cases with too strong peaking of the main ion density profile. The accumulation is due to an inward particle pinch inside the ITB. The peaking increases with the impurity charge and is low for the low-Z elements C and Ne. In the very centre, with low B_p, profiles of T_i, T_e, n_e and n_{Ni} are flat. The dependence of impurity peaking on impurity charge is in agreement with dominant neoclassical impurity transport inside the ITB. Using this assumption, transport modeling yields a good description of the Ne evolution, while the calculated Ni peaking n_{center}/n_{edge} is ≈30% too low.

Acknowledgement:

This work was performed under the European Fusion Development Agreement (EFDA).

References

[1] R. Dux et al., Nucl. Fusion **39**, 1509 (1999).
[2] P. C. Efthimion et al., Nucl. Fusion **39**, 1905 (1999).
[3] R. Dux, et al., in Proc. 28th EUR Conf. Madeira, **25A**(EPS), 505, 2001.
[4] H. Tankenaga and JT-60U team, Phys. Plasmas **8**, 2217 (2001).
[5] W. P. West et al., Phys. Plasmas **9**, 1970 (2002).
[6] R. Dux et al., J. Nucl. Mater. (accepted for publication).
[7] K.-D. Zastrow et al., in Proc. 29th EUR Conf. Montreux, **26B**(EPS), O5.02, 2002.
[8] C. Giroud et al., in Proc. 28th EUR Conf. Madeira, **25A**(EPS), 549, 2001.
[9] H. Chen et al., Nucl. Fusion **41**, 31 (2001).
[10] K.-D. Zastrow et al., in Proc. 26th EUR Conf. Maastricht, **23J**(EPS), 217, 1999.
[11] H. P. Summers, JET-IR 06 (Abingdon: JET Joint Undertaking) (1994).
[12] B. L. Henke, E. M. Gullikson, and J. C. Davis, At. Data and Nucl. Data Tables **54** (1993).
[13] N. C. Hawkes et al., Phys. Rev. Lett. **87**, 115001 (2001).
[14] C. D. Challis et al., Plasma Phys. Controlled Fusion **44**, 1031 (2002).
[15] A. G. Peeters, Phys. Plasmas **7**, 268 (2000).
[16] R. Dux and A. G. Peeters, Nucl. Fusion **40**, 1721 (2000).
[17] S. P. Hirshman and D. J. Sigmar, Nucl. Fusion **21**, 1079 (1981).
[18] F. Crisanti et al., Phys. Rev. Lett. **88**, 145004 (2002).
[19] X. Litaudon et al., Plasma Phys. Controlled Fusion **44**, 1057 (2002).